An objective reconstruction of the Mediterranean sea carbonate system

Tomas Lovato [a,*], Marcello Vichi [a,b,1]

[a] Centro Euro-Mediterraneo sui Cambiamenti Climatici (CMCC), Bologna, Italy
[b] Istituto Nazionale di Geofisica e Vulcanologia (INGV), Bologna, Italy

ABSTRACT

An objective estimation of the current distribution of carbonate system variables for the Mediterranean Sea is proposed using empirical relationships derived from ship-based observations and combined with monthly climatological fields of hydrographic parameters. The high quality data of METEOR84/3 cruise were used to fit multiple linear regression models of Dissolved Inorganic Carbon (DIC) and Total Alkalinity (TA) from other hydrochemical parameters. These algorithms provided a robust estimation of DIC and TA, with corresponding Root Mean Squared Errors of 7.66 and 5.09 μmol/kg, by accounting only for potential temperature, salinity, pressure, and nitrate concentration. After the application of the identified regression models to a set of publicly available climatological fields, an objective assessment of the reconstructed carbonate system monthly distributions was derived and compared against different ship-based surveys. Results showed that the Mediterranean Sea interior was well reproduced with errors < 14 μmol/kg, whereas the near surface layers still exhibited large uncertainties. The lower degree of confidence of this approach at the surface does not allow the direct application for studying anthropogenic CO_2 trends, but some qualitative considerations were drawn from the comparison between the estimated inorganic carbon system and the available observational datasets. Most importantly, the present work showed that the estimated inventories are able to capture the linkages with the physical oceanic features of the system and we propose this method as an inexpensive solution to support the design of monitoring activities in the Mediterranean Sea, which is still poorly constrained by direct observations.

© 2014 Elsevier Ltd. All rights reserved.

1. Introduction

The rise in atmospheric carbon dioxide (CO_2) concentration, primarily caused by human fossil fuel combustion, is tempered by oceanic uptake, which accounts for the removal of nearly a third of anthropogenic carbon added to the atmosphere (Sabine et al., 2004; Doney et al., 2009). The potential storage of anthropogenic CO_2 in the ocean is substantial due to the buffer effect of seawater, as the absorbed CO_2 is partitioned among the components of the carbonic acid, through chemical dissociations, and only a small fraction remains in the undissociated form (Lee et al., 2011). Changes in the distribution of the inorganic carbon inventory are driven by physical advection and mixing of water masses and biological processes (e.g., primary production, remineralization), which contribute to the transfer of anthropogenic CO_2 from the mixed layer toward the ocean interior (Sabine and Tanhua, 2010). A host of

studies have provided a detailed description of inorganic carbon inventories (e.g., Key et al., 2004, 2010; Bakker et al., 2014) and anthropogenic CO_2 storage in open ocean (Khatiwala et al., 2009; Feely et al., 2009; Velo et al., 2013; Khatiwala et al., 2013), but only recently has the scientific interest shifted to the study of marginal seas, as they were recognized to have enormous potential for CO_2 storage (Lee et al., 2011).

The Mediterranean Sea is a semi-enclosed basin characterized by warm, high alkalinity waters, with a fast overturning circulation, thus these waters are capable of absorbing more CO_2 from the atmosphere than the neighbouring oceanic region (Schneider et al., 2010). Experimental evidences (Schneider et al., 2007; Rivaro et al., 2010; Touratier et al., 2012; Álvarez et al., 2014) provided a cross-section distribution of Dissolved Inorganic Carbon (DIC) and Total Alkalinity (TA): an anti-estuarine shallow circulation cell determines an increasing eastward gradient at the surface while maximum values are observed at intermediate depths. Deep waters are characterized by a west to east TA increase of ~ 40 μmol/kg, while the DIC concentrations have a reversed gradient of about 10 μmol/kg.

These available experimental datasets are confined to very short time windows and are not evenly distributed across the

---

basin (Álvarez, 2012). Furthermore, the restricted availability of long-term basin-wide observations of the carbonate system limits our understanding of spatial variability.

Empirical algorithms have generally been used to overcome this lack of direct measurements, in order to derive carbonate system inventories by means of other hydrochemical parameters at both global and regional scales (e.g., Lee et al., 2006; Kim et al., 2010; Plancherel et al., 2013; Evans et al., 2013). This approach works because of the stoichiometric relationships linking carbonate system variations to changes in dissolved oxygen (O_2) and inorganic nutrients (e.g., nitrate and phosphate) and because of the carbonate system thermodynamic dependency on temperature (T), salinity (S), and pressure (P) (e.g., Brewer et al., 1997; Millero, 2007). While not to be considered a substitute for in situ observations, these empirical algorithms offer an inexpensive way of inferring inorganic carbon system data from hydrochemical variables by exploiting their underlying linkages (Juranek et al., 2011; Alin et al., 2012; Bostock et al., 2013).

Different relationships, mainly relying on T, S, and O_2, have been proposed in the literature, with the aims to detect changes in the anthropogenic CO_2 inventory of the Mediterranean Sea (Touratier and Goyet, 2009 and 2011), to identify the key drivers of carbonate system (Schneider et al., 2007), or to extend spatial carbonate data distribution for numerical model development (D'Ortenzio et al., 2008; Louanchi et al., 2009; Taillandier et al., 2012). Despite the growing use of these empirical algorithms approaches, to the best of our knowledge, an objective assessment of their formulations in the Mediterranean Sea is still lacking.

The primary aim of this study is to investigate the spatio-temporal distribution of carbonate system variables in the Mediterranean Sea through the combination of empirical algorithms and observational datasets. An objective statistical method was used to determine optimal multiple linear regression (MLR) models for DIC and TA reconstruction by using the high quality ship-based survey data of the METEOR84/3 cruise (Tanhua et al., 2013). The identified relationships were then applied to the gridded monthly climatologies of hydrochemical parameters produced within the SeaDataNet project (http://www.seadatanet.org) allowing us to produce seasonally varying three-dimensional fields of the carbonate system variables. A comparison with data collected during previous trans-Mediterranean cruises was performed to test the reliability of estimated inorganic carbon variables. Finally, the seasonal spatio-temporal variability of DIC and TA fields were addressed by focusing on the role of major general circulation structures to evaluate their likely involvement in determining the inorganic carbon inventory distributions within Mediterranean waters.

2. Data and methods

2.1. Observational datasets

This study uses the following observational data collected during different trans-Mediterranean ship-based surveys in the last decade (Fig. 1):

1. Meteor 51/2 (M51/2, November 2001), which is assumed in this work to be the oldest cruise describing the distribution of several biogeochemical variables in the Mediterranean Sea. Details on hydrochemical variables sampling and analytical methodologies are given in Schneider et al. (2010).
2. TRANSMED (TMED, May-June 2007) was performed in the framework of the Italian VECTOR project and accounts for major hydrochemical parameters, whereas water samples were analysed only for pH and Total Alkalinity (Rivaro et al., 2010).

Only CTD and carbonate system data have been made available for this work.
3. BOUM (BOUM, June-July 2008) consists of a longitudinal transect with 30 sampling stations which provided information on physical and biogeochemical properties through the entire water column (Moutin et al., 2012; Touratier et al., 2012). Only DIC and TA data from the cruise have been provided for the present study.
4. Meteor 84/3 (M84/3, April 2011) data account for a large variety of hydrographic and biological parameters, as well as a full length and depth description of inorganic carbon variables. Details about the sampling, analysis and quality control are given in Tanhua et al. (2013).

The two Meteor cruises are publicly available at the Carbon Dioxide Information Analysis Center website (http://cdiac.ornl.gov), while TRANSMED and BOUM datasets were kindly made available by partners of the EU project MedSeA (Mediterranean Sea Acidification, Grant agreement 265103).

The monthly climatological fields of temperature, salinity, oxygen and nutrients for the Mediterranean Sea (Pinardi et al., 2007) were obtained from the publicly distributed regional products of the SeaDataNet project (http://www.seadatanet.org/Products). The SeaDataNet infrastructure is primarily involved in data collection and produces integrated databases of standardized quality at global and regional scales. These products are designed to validate and synthetize multidisciplinary datasets relevant to the monitoring of the ocean state and health (Schaap and Lowry, 2010).

These climatologies were constructed through an objective analysis of the observations collected in the period 1890–2002 by using the Data Interpolating Variational Analysis method (DIVA, Troupin et al., 2012). Data are distributed on a regular horizontal grid of $1/8°$ (~ 14 Km) of resolution over 33 vertical levels, with a variable vertical spacing between 0 and 5500 m. Climatological fields of temperature and salinity were obtained using observations homogeneously distributed in space and time, while the lack of observations in deep waters limits the availability of oxygen and nutrients climatological fields along the vertical to maximum depths of 2500 m and ~ 1000 m, respectively.

2.2. MLR models identification

Multiple linear regression methods for the estimation of carbonate system variables were introduced to fill gaps in observational datasets and extend inorganic carbon inventories (e.g., Kim et al., 2010; Juranek et al., 2011; Touratier and Goyet, 2011). In agreement with Friis et al. (2005), it was here assumed that a single empirical algorithm is capable to describe the spatial variability of the carbonate system variables and that the underlying relationships between hydrochemical parameters and inorganic carbon variables do not change over the investigated time frame. These linear relationships primarily describe the natural variability of the system, but in reality deviations are likely to arise due to seasonal changes in hydrochemical properties, especially at the sea surface, or as a consequence of anthropogenic processes over long time scales.

MLR models have the following functional form:

$$Y = \beta_0 + \sum \beta_i \cdot X_i + \varepsilon, \ i = 1, n \qquad (1)$$

where Y is the dependent variable, X_i is the matrix of the n independent variables, β_i indicates an array containing the regression coefficients estimated for each independent variable, with β_0 being the intercept value, and ε is an unexplained random error. The general form accounts only for linear terms, while interaction or quadratic ones are here neglected to limit the enhancement of
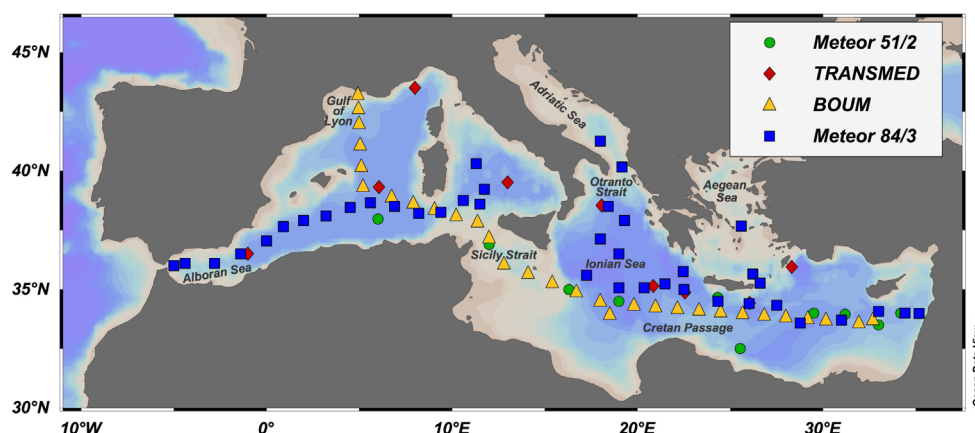
Fig. 1. Distribution of the ship-based surveys performed during Meteor 51/2 (M51/2, circles), TRANSMED (TMED, diamonds), BOUM (triangles), and Meteor 84/3 (M84/3, squares) cruises in the Mediterranean Sea. Only stations where carbonate system variables were collected are shown.

seasonal effects as only a single cruise is used to estimate the MLR models.

Focusing on the independent variables, namely T, S, P, O_2, nitrate (NO_3), phosphate (PO_4), and silicate (SiO_2), MLR models for DIC and TA were determined using the data collected throughout the full water column during the oceanographic survey of the most recent and extensive M84/3 cruise within the Mediterranean Sea (stations across and outside the Gibraltar Strait were not included, see Fig. 1). According to the existing literature (Aït-Ameur and Goyet, 2006; Tanhua et al., 2007; Touratier and Goyet, 2009), potential temperature (θ) and Apparent Oxygen Utilization (AOU) were also used to develop similar empirical algorithms. Consequently, these parameters were derived using the Gibbs Seawater Oceanographic Toolbox (McDougall and Barker, 2011) and included in the set of independent variables.

An objective statistical assessment method was implemented to select the optimal combination of hydrochemical variables for the model structure: i) different MLR models were determined through a stepwise regression procedure; ii) the root mean squared error (RMSE) was computed as a measure of each model performance; iii) multiple collinearity among independent variables was detected using the Variance Inflation Factor (VIF, Hair et al., 2009).

The VIF statistic is a measure of the increasing linear dependence between two or more parameters, which indicate an unstable estimate of regression coefficients. As suggested by Hair et al. (2009), a VIF maximum threshold value of 5 was adopted.

The MLR model that yielded to a minimum RMSE, with independent variables exhibiting VIF values below the chosen threshold, was considered optimal.

In addition, an explicit quantification of the relative importance of each independent variable (RI_X) included in optimal MLR models was determined using the method proposed by Lindeman et al. (1980). This variance decomposition technique determines the proportion of variance explained by each linear regressor and it overcomes the limitations of standard methods due to the presence of linear dependence among variables (Grömping, 2006).

2.3. Estimation of the spatio-temporal distribution of DIC and TA

The identified optimal MLR models for DIC and TA were used to compute their spatio-temporal distribution using the SeaDataNet monthly climatological datasets as input fields.

Since the objective procedure used to generate these climatologies prevents the interpolation below a critical data density (Troupin et al., 2012), some gaps were present in oxygen and nutrients data, especially in intermediate and deep layers. A linear piecewise interpolation was used to fill temporal gaps over populated grid

nodes with at least ten monthly values, without performing further extrapolations (as for instance along the vertical) to avoid large divergences from the original dataset.

The consistency of estimated DIC and TA monthly climatologies was tested through the comparison with the four available ship-based oceanographic surveys (see Section 2.1). Although a better agreement is expected for the M84/3 data that were used to derive the MLRs, this dataset was here retained to enable for the detection of potential deviations that may arise when the independent variables comes from the climatological fields. In this step, each cruise was associated to a specific month by taking the one with the largest number of sampled stations. The location of each sampling station was mapped over the gridded dataset using a single point nearest-neighbour method, while a linear interpolation was performed to extract the vertical profiles at the same depths of the observed data.

A statistical analysis of the reconstructed vs. observed datasets was carried out to quantify data variability and biases over different time windows and along the water column. This analysis included the following descriptive statistics and error metrics: sample total pairs, Mean Bias Error (MBE), Mean of Absolute Errors (MAE), RMSE, the ratio between observed and reconstructed coefficients of variation (CVR), and the non-parametric correlation coefficient of Spearman (r_s).

Although RMSE is widely adopted as an error indicator for inter-comparison exercises, it was shown by Willmott and Matsuura (2005) that this metric might easily lead to misinterpretations of the real error distribution and MAE is indicated as the most natural measure of average error magnitude. Therefore, we reported RMSE for consistency with previous scientific works, but MAE was here assumed as the reference metric for the uncertainty estimation. These two metrics were computed also for the data pairs below 400 m to enable for the additional comparison with previous literature findings (e.g., Schneider et al., 2007; Touratier and Goyet, 2009), which developed similar empirical relationships using only observations below a specific depth threshold, like the annual mean mixed layer depth. The CVR was also introduced as an indicator of the variability between reconstructed and observed data to assess the error of the estimated fields.

3. Results

3.1. Optimal MLR model identification and carbonate system variable estimates

From the data collected throughout the full water column during the M84/3 cruise, a set of hydrochemical parameters (T, S, P, O_2, NO_3,

Table 1
Summary of the optimal MLR models for DIC and TA identified using the M84/3 cruise dataset (see Eq. 1). The relevant column-wise statistics are: total samples (n), Variance Inflation Factor (VIF), relative importance of independent variables (RI_X, %), linear regression coefficients (β) and standard error (SE), determination coefficient (R^2) and RMSE values (μmol/kg). Alternative models obtained in the stepwise regression procedure are also reported, including three combinations of independent variables with the lower RMSE values and a simple one with only θ and S. For these models are indicated the R^2 and RMSE metrics and the VIF value associated to each variable.

Y	Stepwise R^2, RMSE	X	VIF	RI_X	β	SE
DIC	0.96, 7.66	Intercept			$3.57 \cdot 10^1$	$4.74 \cdot 10^1$
(n=704)		θ	4.63	17.3	$-1.16 \cdot 10^1$	$9.20 \cdot 10^{-1}$
		S	1.06	58.3	$6.26 \cdot 10^1$	$1.25 \cdot 10^0$
		P	1.53	3.5	$-5.37 \cdot 10^{-3}$	$7.50 \cdot 10^{-4}$
		NO$_3$	3.82	20.9	$3.87 \cdot 10^0$	$3.75 \cdot 10^{-1}$
Alternative models (R^2; RMSE; VIF)						
θ, S, P, NO$_3$, AOU: 0.96; 7.49; 5.2, 1.4, 1.6, 7.0, 6.9				θ, S, P, PO$_4$: 0.96; 7.89; 3.4, 1.0, 1.5, 2.8		
θ, S, P, AOU: 0.94; 9.44; 4.6, 1.4, 1.6, 3.8				θ, S: 0.92; 10.90; 1.0, 1.0		
TA	0.98, 5.09	Intercept			$-6.33 \cdot 10^2$	$3.17 \cdot 10^1$
(n=688)		θ	4.52	1.1	$-7.67 \cdot 10^0$	$6.17 \cdot 10^{-1}$
		S	1.06	95.7	$8.67 \cdot 10^1$	$8.31 \cdot 10^{-1}$
		P	1.52	2.3	$5.01 \cdot 10^{-4}$	$5.04 \cdot 10^{-4}$
		NO$_3$	3.74	0.8	$-1.97 \cdot 10^0$	$2.48 \cdot 10^{-1}$
Alternative models (R^2; RMSE; VIF)						
θ, S, P, NO$_3$, AOU: 0.98; 5.11; 5.0, 1.4, 1.6, 7.0, 6.8				θ, S, P, PO$_4$: 0.98; 5.29; 3.4, 1.0, 1.5, 2.7		
θ, S, P, AOU: 0.98; 5.59; 4.4, 1.3, 1.6, 3.6				θ, S: 0.98; 6.03; 1.0, 1.0		

PO$_4$, SiO$_2$, θ, and AOU) was tested through the objective approach described in Section 2.1 to identify the combination of variables with the highest predictive power to estimate DIC and TA.

The set of the independent variables θ, S, P, and NO$_3$ yielded the optimal MLR models for DIC and TA, with corresponding RMSE values of 7.66 and 5.09 μmol/kg and R^2 of 0.96 and 0.98 (Table 1). Values of VIF were less than 5 for all terms of the linear regression algorithms, indicating that there was no critical collinearity between the independent variables. The variance decomposition of the optimal MLR models indicates that salinity contributed for 95.7% of the TA explained variance, while a composite structure emerged for the DIC model, where the summed contribution of salinity, θ, and NO$_3$ was equal to 96.5%. Using the independent variables analytical precision (δx) of the M84/3 cruise ($\delta_\theta = \pm 0.002$ °C, $\delta_S = \pm 0.003$, $\delta_P = \pm 0.015\%$dbar, $\delta_{NO3} = \pm 0.08$ μmol/kg, see Tanhua et al. (2013)) and their propagation in the optimal MLR models (Table 1), the expected prediction error for DIC and TA was of 7.1 and 9.2 μmol/kg, respectively.

Alternative models obtained in the stepwise regression procedure are also reported in Table 1, accounting for three combinations of independent variables with low RMSE values and a simple one with only θ and S. These models showed varying degrees of error, especially for DIC. In particular, the addition of AOU resulted in a slightly better MLR model for DIC (RMSE=7.49 μmol/kg), but it was discarded due to the high collinearity between AOU, NO$_3$, and potential temperature, being the related VIF > 5.

These optimal regression models were then used to estimate the spatio-temporal distributions of DIC and TA using the SeaDataNet monthly climatologies as input fields. The application of the empirical algorithms was limited to a maximum depth of about 1000 m to cope with the data availability of nitrate climatologies (see Section 2.1). A general overview of the carbonate variables reconstruction in the epi- and mesopelagic Mediterranean waters and of the input hydrochemical variables is illustrated in Fig. 2, showing the annual mean vertical distributions along an eastward cross-basin section.

In the near-surface layers, DIC concentrations varied between 2110 and 2240 μmol/kg according to a west to east gradient that vanishes close to 250 m depth (Fig. 2a). The western and eastern basins exhibited higher concentrations at intermediates depths (500–1000 m) with mean values of about 2320 and 2315 μmol/kg, respectively. In particular, the vertical distribution of DIC in the eastern Mediterranean presents two maxima between 500 and

750 m at the opposite sides of the sub-basin, while lower concentrations were obtained along the Cretan passage.

The basin wide distribution of TA at the surface is characterized by a gradient similar to that of DIC, with concentrations increasing from $\sim$2400 μmol/kg in the approaches of the Gibraltar Strait up to 2600 μmol/kg at the opposite side of the basin (Fig. 2b). Contrarily to DIC, the west–east gradient is preserved along the vertical section but its magnitude decreases rapidly toward deeper layers, with a difference of about 30 μmol/kg around 500 m. At intermediate depths, the mean concentration in the Western Mediterranean (2585 μmol/kg) is remarkably different from the one obtained in the Eastern Mediterranean (2612 μmol/kg). The vertical distribution of both estimated carbonate variables is characterized by very low concentrations between 500 and 1000 m along the Sicily Strait, which are more visible in the case of DIC section profile.

3.2. Assessment of the DIC and TA reconstructed fields

A reconstruction of the four ship-based oceanographic surveys was achieved through a mapping procedure of the observed profiles over the estimated spatio-temporal distributions of DIC and TA (see details in Section 2.3).

The results of reconstructed vs. observed data comparison in the epi- and mesopelagic Mediterranean waters are summarized by means of different descriptive statistics and error metrics in Table 2. The reconstruction of DIC and TA is generally characterized by negative biases (indicated by the MBE descriptor) in all cruises but M51/2 and, not surprisingly, the lowest values resulted for the M84/3 dataset. Mean absolute errors of the estimated DIC field were larger than TA ones, being the respective average MAE equal to 18 and 14.3 μmol/kg. The largest values of MAE and RMSE for both inorganic carbon variables were obtained for the two summer cruises, namely TMED and BOUM. The ratio of the coefficient of variations addresses the precision of the reconstructed fields in term of variability. The lowest, but still satisfactory, CVR values were obtained for the M84/3 cruise, which also has the largest amount of data pairs, while values close to 1 were obtained for the other datasets. The non-parametric Spearman correlation was statistically significant and larger than 0.6 for all the reconstructed cruises, with higher values for BOUM and M84/3. The RMSE and MAE statistics computed for the data pairs below 400 m exhibited a better agreement with observations, especially for TA, with values that were two to three times smaller than those computed for the entire water column.
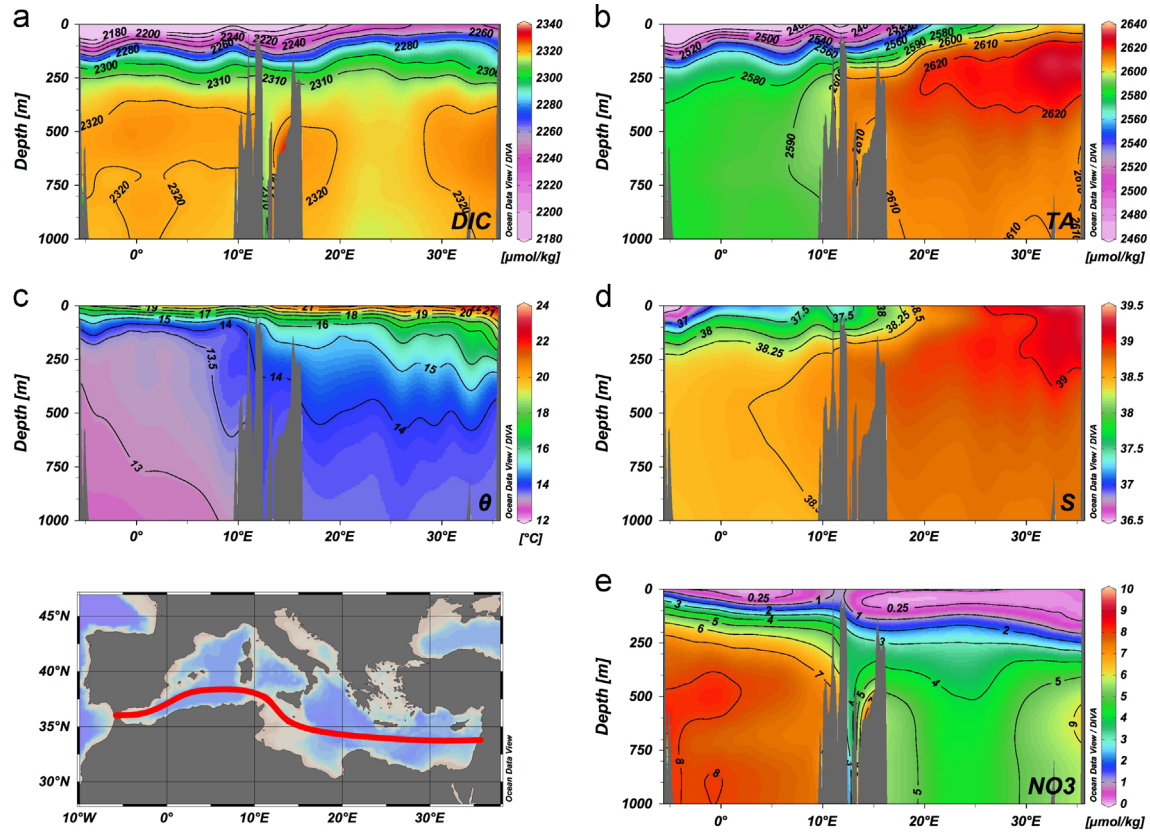
Fig. 2. Annual mean vertical distribution of estimated Dissolved Inorganic Carbon (a) and Total Alkalinity (b), and input fields for potential temperature (c), salinity (d), and nitrate (e) along a west to east section of the Mediterranean Sea. The cross-basin section indicated in the map is 25 km wide. DIC and TA fields were computed using the optimal MLR models of Table 1. Carbonate system variables were plotted using a linear interval but with a non-linear colourmap to illustrate the large range of variability.

Table 2
Statistics of the reconstructed vs. observed DIC and TA data for the four available ship-based oceanographic surveys (see Section 2.1). The location of sampling point over the gridded fields is described in Section 2.3. The adopted metrics are: reference month, sample total pairs, Mean Bias Error of the reconstructed vs. observed data (MBE, μmol/kg), Root Mean Squared Error (RMSE, μmol/kg), Mean of Absolute Errors (MAE, μmol/kg), RMSE and MAE for data pairs below 400 m, the ratio between the coefficients of variation of observed and reconstructed data (CVR), and Spearman correlation). (r_s). Bold type indicates statistical significance with p-value < 0.05. Note that direct observations of DIC were not available for TMED cruise. The analytical precision (δ_X, μmol/kg) of DIC and TA measurements for each cruise is also reported.

	Month	Pairs	δ_X	MBE	RMSE	MAE	RMSE$_{400}$	MAE$_{400}$	CVR	r_S
DIC										
M51/2	11	251	1.5[a]	8.76	22.66	17.08	13.18	12.03	1.03	**0.67**
TMED	–	–	–	–	–	–	–	–	–	–
BOUM	6	567	2[c]	−11.69	32.12	23.05	11.54	9.00	1.02	**0.81**
M84/3	4	735	2.5[d]	−1.73	18.34	13.39	7.84	6.44	0.80	**0.74**
TA										
M51/2	11	250	4.2[a]	8.49	15.85	12.77	10.29	8.98	1.10	**0.62**
TMED	6	138	4[b]	−2.84	23.95	15.77	6.45	5.24	0.88	**0.67**
BOUM	6	423	4[c]	−6.28	22.71	16.94	10.58	8.67	0.97	**0.89**
M84/3	4	722	1[d]	−0.22	15.47	10.02	5.54	4.18	0.84	**0.92**

[a] Schneider et al. (2010).
[b] Rivaro et al. (2010).
[c] Moutin (2010).
[d] Tanhua et al. (2013).

Fig. 3 depicts the vertical distributions of the MAE for DIC and TA computed over discrete depth intervals for each ship-based survey, together with the corresponding mean values. The mean value of MAEs significantly decreased form the surface to intermediate layers, with values in the range 10–15 μmol/kg below 200 m, while the largest differences were located in the upper layer (0–50 m), especially when comparing against the two summer cruises (TMED and BOUM). The overall distribution of

DIC errors was rather similar among the four cruises (Fig. 3a), while significant variability characterized the reconstruction of Total Alkalinity (Fig. 3b). In particular, the MAE values of TA for the three more recent cruises were within the range of 5 μmol/kg, whereas between 500 and 600 m BOUM values exhibited a high RMSE value. It clearly emerged that errors calculated from M51/2 cruise were systematically larger than those of the M84/3 ones for both inorganic carbon variables.
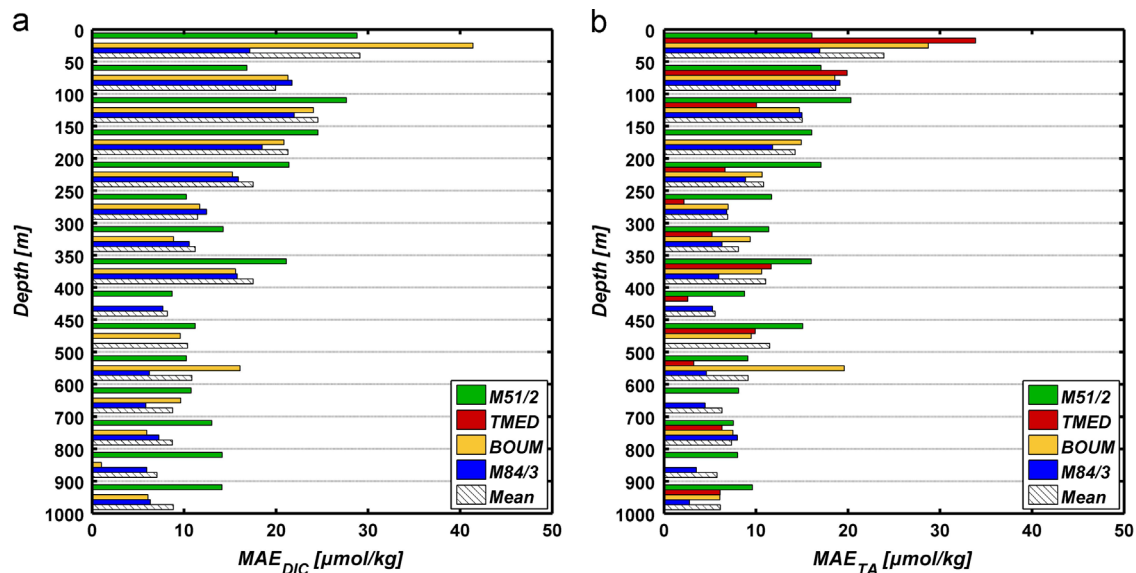
Fig. 3. Distribution of Mean Absolute Error (MAE) values computed for DIC (a) and TA (b) over discrete depth intervals for the available trans-Mediterranean ship-based surveys (see Fig. 1 for details and stations location) and the mean values computed from the available datasets (hatched bars). The location of sampling point over the gridded fields is described in Section 2.3. Note that during the TMED cruise DIC data were not collected.

4. Discussion

4.1. Relevance of the estimated DIC and TA fields

In the first step of this work, an objective procedure was used to determine optimal MLR models for DIC and TA by exploiting high quality data collected during the M84/3 trans-Mediterranean cruise. The error of the optimal MLR models for DIC (7.66 μmol/kg) and TA (5.09 μmol/kg) was comparable to that obtained in previous works using similar empirical algorithms (see, e.g., Schneider et al., 2007; Rivaro et al., 2010; Touratier et al., 2012). In particular, the propagation of the analytical precision into the optimal MLR models indicated that uncertainties were nearly the half of the MAE values computed over the entire water column, but they were closer to the MAE errors computed considering only data below 400 m.

The variance decomposition analysis of Section 3.1 showed that salinity and potential temperature explain up to 75.6% of the DIC variability with a significant contribution of nitrate (20.9%), while the bulk of TA variability is related to salinity ($RI_S = 95.7$%). This result indirectly suggests that spatio-temporal changes in the biological processes of the system play an integral role in the distribution of DIC within the Mediterranean Sea.

On such a basis, the extension of the optimal MLR models to the SeaDataNet monthly climatological fields for θ, S, P, and NO_3 was carried out to estimate the carbonate system characteristic in the Mediterranean Sea (see Section 2.3). The horizontal and vertical gradients of the cross-basin annual vertical profiles (Fig. 2) compared well with those reported by Álvarez et al. (2014), whereas the absolute difference in DIC concentration between west and east at intermediate depths was ~5 μmol/kg lower. Local discontinuities were detected in the Sicily Strait area and along the eastern Mediterranean coast, especially for DIC (Fig. 2a), which may be attributed to the sparse distribution of raw data used for the input climatological fields, more likely NO_3. These discrepancies can be explained by assuming that data outliers were not detected by the quality analysis procedure before the interpolation of the SeaDataNet hydrographic climatologies (Pinardi et al., 2007).

The reconstruction of DIC and TA data through the extension of empirical relationships provides useful baseline insights, although

the direct application as a reference dataset for the carbonate system distribution in the Mediterranean Sea should be considered with due care. The error analysis carried out in Section 3.2 represents an initial robust validation of this climatological inventory, and it should be considered as a measure of the associated uncertainty in all utilizations of this reconstructed dataset. An alternative evaluation of the uncertainty would involve the use of the relative errors computed by the DIVA algorithm (see Troupin et al., 2012), but it is not yet applicable since the scarcity of nitrate data leads to significantly high uncertainties in the interpolation procedure.

The comparison of the observed profiles with the ones mapped over the estimated carbonate fields for the four ship-based surveys leads to MAEs equal to ~1% and ~0.05% of the averaged concentrations in the Mediterranean Sea for DIC and TA, respectively. Moreover, the accuracy of reconstructed concentrations in the ocean interior (below 400 m) was still comparable to those of the optimal MLR models, but of course higher than the analytical precision of inorganic carbon measurements (see Table 2). Thus, the determination of carbonate system variables using surface to bottom data provides a good representation of intermediate waters and an acceptable description of their characteristics also in upper layers, at the cost of slightly higher uncertainties (see e.g., Friis et al., 2005; Evans et al., 2013). Near-surface data are affected by larger biases as a consequence of combined, uncertain physicochemical process (Brewer et al., 1995; Orr et al., 2005; Millero, 2007), as clearly seen in the reconstruction of the cruises performed during the summer season (Fig. 3). The regression algorithms exhibited limited skills in surface waters possibly because they were estimated using only one observational dataset for April, since the underlying relationships between dependent and independent variables may assume different weights in response to the seasonal variability of sea temperature and biological cycles. The combination of repeated oceanographic surveys, i.e. with high temporal frequency, would lead to a more robust assessment of the carbonate system variability in the upper water column (see, e.g., Alin et al., 2012). It is indeed reasonable to assume that the estimated DIC and TA climatological fields describe a local condition of the system, which closely reflects that of the cruise employed to derive the empirical relationships. A larger set of observational data over time is also required to ensure the

construction of carbonate climatological fields with an extended temporal validity (see, e.g., Bostock et al., 2013).

The proposed climatologies are central to the estimate of carbonate system distribution within Mediterranean waters, but a quantitative assessment of the anthropogenic CO_2 accumulation is here precluded because both statistical and analytical uncertainties are on the same order of the CO_2 penetration signal. Nevertheless, it is possible to draw some qualitative considerations from the error analysis of M84/3 and M51/2 cruises that were carried out at 10-year time difference. The first one was used to design the MLR models and, as expected, the statistical analysis of the reconstructed data coherently exhibited the smaller error metrics (Table 2). Conversely, the MBE of the M51/2 cruise were the highest for both DIC and TA, while error deviation and mean absolute errors were rather similar to those obtained for M84/3. This resemblance in the error dispersion can be associated to the effect of common physical and biological processes that contribute to the carbonate system distribution. Bearing in mind that the two cruises were performed ten years apart, the increase of DIC and TA concentrations throughout the water column can be attributed to the combined effect of the overturning circulation variability (Schneider et al., 2014), the intense evaporative processes within the basin (Borghini et al., 2014; Cardin et al., 2014), and the penetration of atmospheric CO_2 toward the intermediate waters (Touratier and Goyet, 2009).

4.2. Linkages between the carbonate system and circulation structures

The spatio-temporal variability of the estimated DIC and TA fields can be addressed by focusing on the Mediterranean intermediate waters.

The horizontal spatial distribution of annual averaged DIC and TA fields at the bottom of the winter mixing layer (~250 m) and within intermediate waters (750 m) are illustrated in Fig. 4. As seen with the cross-basin section analysis (see Section 3.1), DIC is characterized by a small west to east gradient at intermediate depth, while TA presents a large variation from the low Alboran Sea concentrations to the higher ones of the Aegean Sea. As previously highlighted, DIC estimates are affected by marked discontinuities in the approaches of Sicily and Otranto Straits that are not clearly attributable to distinct physical or biological processes.

Several features emerge from the DIC and TA distributions at 250 m (Fig. 4, top panels): large-scale circulation structures are visible in the Gulf of Lyon and in the Central Mediterranean Sea; the exchanges with the Atlantic waters in the western Mediterranean Sea are clearly recognizable in the low TA signal; most of the relevant sub-basin scale cyclonic and anticyclonic circulation structures can be detected, such as the Ierapetra, Rhodes, and Shikmona gyres (cf. Pinardi et al. (2013) for their location). High DIC concentrations characterize the area of the Gulf of Lion and the Southern Adriatic and Rhodes gyres. This tight linkage between carbonate system variable distributions and known circulations features of the Mediterranean Sea is not trivial, as empirical relationships were computed without accounting for the spatial distribution of the observed data.

Most of the sub-surface circulation features are not recognizable in the spatial distribution of the carbonate variables at 750 m (Fig. 4, bottom panels), which are instead characterized by largely homogeneous DIC values and a reduced west to east gradient of TA. The persistence of this gradient indicates that the reconstructed field captures also the high alkalinity pattern of intermediate waters outflowing form the Eastern Mediterranean basin (Schneider et al., 2007).

The seasonal evolution as estimated by the DIC and TA reconstructions was further addressed by focusing on the vertical variability of the Rhodes cyclonic gyre and Pelops anticyclonic eddy (Fig. 5). These regions were selected because of the marked DIC and TA changes in the upper water column, with particularly low concentrations for both carbonate variables in the Pelops anticyclone (see Fig. 4). The uncertainty associated to the estimated carbonate variables is given by the mean value of MAEs for the available ship-based surveys at regular 100 m depth-intervals (Fig. 5e,f).

The largest discrepancy between observations and reconstructed data occurred at the surface layer, with errors larger than 20 μmol/kg (see also Fig. 3). In the case of DIC, this uncertainty might be related to the seasonal variability of primary production processes, which is partly captured by the correlation with the nitrate climatology. The significant reduction of surface TA values during the summer period is instead artificial, since the strong evaporation that takes place in this season determines an increase of alkalinity concentrations (Schneider et al., 2007).

As pointed out in the previous Section, the extension of empirical algorithms to temporal windows beyond that of the data used for the linear model construction may lead to inconsistencies. The
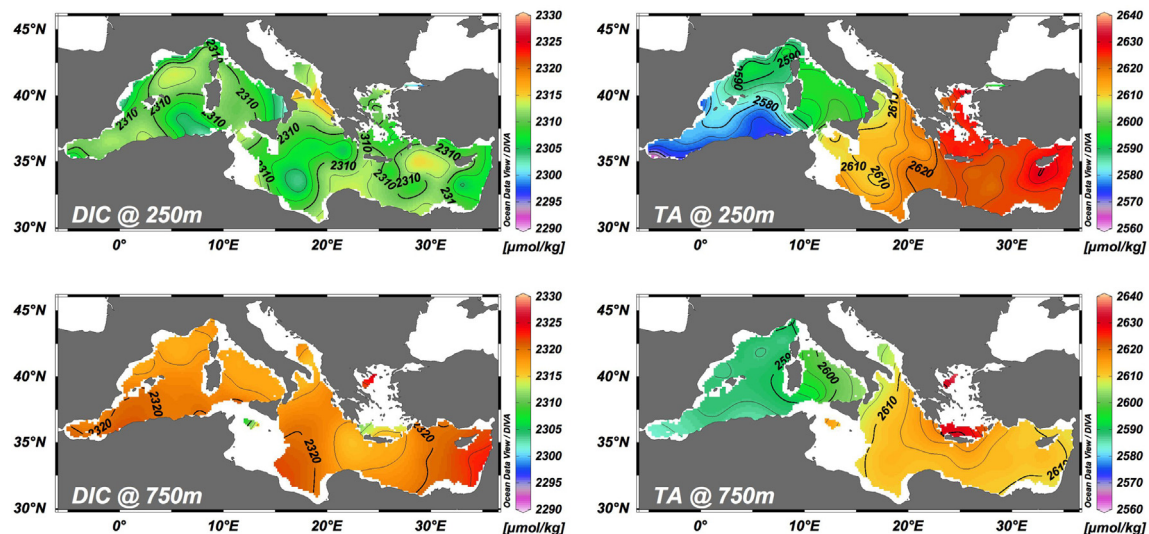

Fig. 4. Basin-wide spatial distribution of the estimated DIC and TA annual fields at 250 (upper panels) and 750 (lower panels) metres depth. Unlabelled contours have an interval of 2.5 μmol/kg.
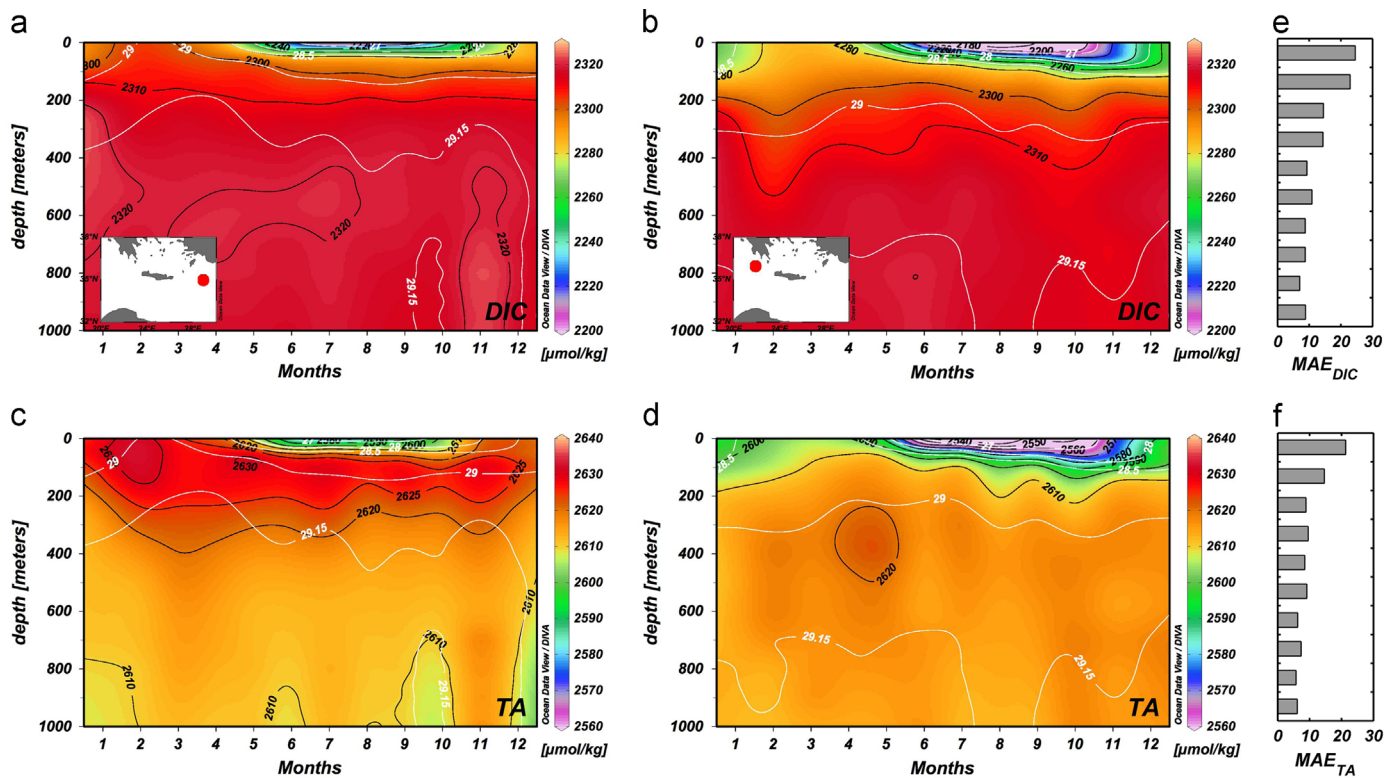
Fig. 5. Temporal evolution of DIC and TA vertical profiles down to 1000 metres for the two selected regions: Rhodes cyclone (a, c), and Pelops anticyclone (b, d). Overlain are the potential density anomaly isolines (kg/m³, white colour). The uncertainty associated to every 100 m depth-interval is indicated through the averaged DIC (e) and TA (f) MAE values for the available ship-based surveys (see also Fig. 3).

concurrent use of error estimates is by far the best way to establish a degree of confidence for an appropriate analysis of the reconstructed DIC and TA fields.

The low MAEs associated with the layers below the surface allow us to infer the linkage between circulation structures and carbonate system seasonal evolution. The upwelling process of the Rhodes cyclonic gyre, more intense during the winter period generates and upward shift of the iso-concentration lines, i.e. the 2300 μmol/kg DIC isoline is located at approximately 100 m (Fig. 5a), while the same one is closer to 200 m of depth in the cross-basin section (Fig. 2a). In particular, the vertical distribution of DIC varies with the potential density anomaly, being the isolines of 2300 μmol/kg and 29 kg/m³ very close and both showing a winter surface outcropping. Beside the spurious concentration decrease of TA in the very surface layers, the highest values were obtained around 100 m depth as expected, due to the dominance of evaporation processes in the upper water column. According to the present empirical reconstruction, TA exhibits more homogeneous values at intermediate depths, but the seasonal shifting of iso-concentration lines showed a weaker connection with that of the density field.

The Pelops anticyclone (inset in Fig. 5b) was described as a semi-permanent eddy or a recurrent gyre of the Mediterranean Sea (Pinardi et al., 2013) that is characterized by weak intermittent downwelling processes. The reconstruction method is able to capture the main features that are expected to dominate in this region. The DIC isoline of 2300 μmol/kg is centred at ∼200 m with alternate deepening phases throughout the year and it varies coherently with the isopycnal horizon equal to 29 kg/m³. Contrarily to the Rhodes gyre, a similar pattern can be recognized also for TA when considering the location of the 2610 μmol/kg iso-concentration line (Fig. 5d).

The emergence of distinctive Mediterranean Sea circulation patterns in the estimated carbonate system fields is a consequence of the large variance contribution of temperature and salinity that is a result of the applied MLR model (Table 2). However, the coherent existence of structures in the carbonate variables hints at a strong underlying relationship between physical, chemical, and biological processes.

5. Conclusions

An objective approach was proposed to determine the spatial and seasonal distribution of principal carbonate system variables in the epi- and mesopelagic Mediterranean waters by combining empirical algorithms and climatological fields of different hydrochemical parameters.

The indirect estimation of DIC and TA distributions allowed us to extrapolate spatio-temporal features over the whole domain, as well as to describe the seasonal evolution of the inorganic carbon system in relation to sub-basin scale cyclonic and anticyclonic circulation structures in the Eastern Mediterranean Sea. Far from being a replacement of ship-based surveys, these empirical inventories represent an inexpensive solution to quickly support the design of future monitoring activities and maximize the value of direct measurements. The addition of limited number of new observations collected in areas with characterizing circulation structures like the Pelops or Rhodes gyres is expected not only to improve the overall description of the carbonate system in the Mediterranean Sea, but also to increase the reliability of empirical estimates, thus improving their degree of confidence in other data-poor regions. Our analysis has also highlighted the need to

extend the number of measurements in the major connecting straits such as Otranto and the Sicily Straits.

An assessment of the errors associated to the reconstructed carbonate system fields was proposed through the use of the Mean Absolute Errors metric. The uncertainty values were low in the ocean interior, while higher values were obtained for the near surface layers. Even if the reliability in the upper water column may preclude a direct computation of anthropogenic CO_2 penetration rates, the estimated carbonate system data can be profitably exploited as input fields for numerical models, since the shorter time scales of upper ocean processes allow for a quick adjustment of the initial conditions.

The realization of a Mediterranean Sea carbonate system data synthesis, such as CARINA and PACIFICA projects (http://cdiac.ornl.gov/oceans/), represents a key step in order to advance our knowledge of inorganic carbon distribution in this region. Moreover, the realization of a similar inventory will allow to improve the approach presented in this work and support the extension of these indirect estimation methods to other relevant parameters such as pH and carbonate saturation horizons.

Acknowledgements

References

Aït-Ameur, N., Goyet, C., 2006. Distribution and transport of natural and anthropogenic CO_2 in the Gulf of Cádiz. Deep Sea Res. II: Topical Stud. Oceanogr 53 (11), 1329–1343.

Alin, S.R., Feely, R.A., Dickson, A.G., Hernández-Ayón, J.M., Juranek, L.W., Ohman, M.D., Goericke, R., 2012. Robust empirical relationships for estimating the carbonate system in the southern California current system and application to CalCOFI hydrographic cruise data (2005–2011). J. Geophys. Res. Oceans (1978–2012) 117 (C5).

Álvarez, M., 2012: The CO_2 system observations in the Mediterranean Sea: past, present and future. In: Briand, F. (Ed.), CIESM, Designing Med-SHIP: A Program for Repeated Oceanographic Surveys. CIESM Workshop monographs 43, Monaco, pp. 164.

Álvarez, M., Sanleón-Bartolomé, H., Tanhua, T., Mintrop, L., Luchetta, A., Cantoni, C., Schroeder, K., Civitarese, G., 2014. The CO_2 system in the Mediterranean Sea: a basin wide perspective. Ocean Sci 10, 69–92.

Bakker, D.C.E., Pfeil, B., Smith, K., Hankin, S., Olsen, A., et al., 2014. An update to the Surface Ocean CO2 Atlas (SOCAT version 2). Earth Syst. Sci. Data 6, 69–90.

Borghini, M., Bryden, H., Schroeder, K., Sparnocchia, S., Vetrano, A., 2014. The Mediterranean is becoming saltier. Ocean Sci 10, 693–700.

Bostock, H.C., Fletcher, S.E., Williams, M.J.M., 2013. Estimating carbonate parameters from hydrographic data for the intermediate and deep waters of the Southern Hemisphere Oceans. Biogeosciences 10, 6199–6213.

Brewer, P.G., Glover, D.M., Goyet, C., Shafer, D.K., 1995. The pH of the North Atlantic Ocean: Improvements to the global model for sound absorption in seawater. J. Geophys. Res. Oceans (1978–2012) 100 (C5), 8761–8776.

Brewer, P.G., Goyet, C., Friederich, G., 1997. Direct observation of the oceanic CO_2 increase revisited. Proc. Natl. Academy Sci 94 (16), 8308–8313.

Cardin, V., Civitarese, G., Hainbucher, D., Bensi, M., Rubino, A., 2014. Thermohaline properties in the Eastern Mediterranean in the last three decades: is the basin returning to the pre-EMT situation? Ocean Sci. Discussion 11, 391–423.

D'Ortenzio, F., Antoine, D., Marullo, S., 2008. Satellite-driven modeling of the upper ocean mixed layer and air–sea CO_2 flux in the Mediterranean Sea. Deep Sea Res. I: Oceanogr. Res. Papers 55 (4), 405–434.

Doney, S.C., Fabry, V.J., Feely, R.A., Kleypas, J.A., 2009. Ocean acidification: the other CO_2 problem. Marine Sci 1, 169–192.

Evans, W., Mathis, J.T., Winsor, P., Statscewich, H., Whitledge, T.E., 2013. A regression modeling approach for studying carbonate system variability in the northern Gulf of Alaska. J. Geophys. Res. Oceans 118 (1), 476–489.

Feely, R.A., Doney, S.C., Cooley, S.R., 2009. Ocean acidification: present conditions and future changes in a high-CO_2 world. Oceanography 22 (4), 36–47.

Friis, K., Körtzinger, A., Pätsch, J., Wallace, D.W., 2005. On the temporal increase of anthropogenic CO_2 in the subpolar North Atlantic. Deep Sea Res. I: Oceanogr. Res. Papers 52 (5), 681–698.

Grömping, U., 2006. Relative importance for linear regression in R: the package relaimpo. J. Statistical Softw 17 (1), 1–27.

Hair, J.F., Black, W.C., Babin, B.J., Anderson, R.E., 2009. Multivariate Data Analysis, seventh ed Pearson Prentice Hall, Upper Saddle River, NJ p. 760.

Juranek, L.W., Feely, R.A., Gilbert, D., Freeland, H., Miller, L.A., 2011. Real-time estimation of pH and aragonite saturation state from Argo profiling floats: prospects for an autonomous carbon observing strategy. Geophys. Res. Lett 38 (17), 1–7.

Key, R.M., Kozyr, A., Sabine, C.L., Lee, K., Wanninkhof, R., Bullister, J.L., Feely, R.A., Millero, F.J., Mordy, C., Peng, T.-H., 2004. A global ocean carbon climatology: results from Global Data Analysis Project (GLODAP). Glob. Biogeochem. Cycles 18, GB4031.

Key, R.M., Tanhua, T., Olsen, A., Hoppema, M., Jutterström, S., Schirnick, C., van Heuven, S., Kozyr, A., Lin, X., Velo, A., Wallace, D.W.R., Mintrop, L., 2010. The CARINA data synthesis project: introduction and overview. Earth Syst. Sci. Data 2, 105–121.

Khatiwala, S., Primeau, F., Hall, T., 2009. Reconstruction of the history of anthropogenic CO_2 concentrations in the ocean. Nature 462 (7271), 346–349.

Khatiwala, S., Tanhua, T., Mikaloff Fletcher, S., Gerber, M., Doney, S.C., Graven, H.D., Gruber, N., McKinley, G.A., Murata, A., Ríos, A.F., Sabine, C.L., 2013. Global ocean storage of anthropogenic carbon. Biogeosciences 10, 2169–2191.

Kim, T.W., Lee, K., Feely, R.A., Sabine, C.L., Chen, C.T.A., Jeong, H.J., Kim, K.Y., 2010. Prediction of Sea of Japan (East Sea) acidification over the past 40 years using a multiparameter regression model. Glob. Biogeochem. Cycles 24 (3), 1–14.

Lee, K., Sabine, C.L., Tanhua, T., Kim, T.W., Feely, R.A., Kim, H.C., 2011. Roles of marginal seas in absorbing and storing fossil fuel CO_2. Energy Environ. Sci 4 (4), 1133–1146.

Lee, K., Tong, L.T., Millero, F.J., Sabine, C.L., Dickson, A.G., Goyet, C., Park, G.-H., Wanninkhof, R., Feely, R.A., Key, R.M., 2006. Global relationships of total alkalinity with salinity and temperature in surface waters of the world's oceans. Geophys. Res. Lett. 33 (19), 1–5.

Lindeman, R.H., Merenda, P.F., Gold, R.Z., 1980. Introduction to bivariate and multivariate analysis. Foresman & Co; Glenview, IL, Scott, p. 444.

Louanchi, F., Boudjakdji, M., Nacef, L., 2009. Decadal changes in surface carbon dioxide and related variables in the Mediterranean Sea as inferred from a coupled data-diagnostic model approach. ICES J. Mar. Sci.: J. du Conseil 66 (7), 1538–1546.

McDougall, T.J., Barker, P.M., 2011. Getting started with TEOS-10 and the Gibbs Seawater (GSW) Oceanographic Toolbox, SCOR/IAPSO WG127, 28pp., isbn:978-0-646-55621-5.

Millero, F.J., 2007. The marine inorganic carbon cycle. Chem. Rev 107 (2), 308–341.

Moutin, T., 2010. BOUM cruise – Protocols for sampling and analysis. BOUM Cruise Documentation, 24 ⟨http://www.mio.univ-amu.fr/BOUM⟩ (accessed 01.11.2014).

Moutin, T., Van Wambeke, F., Prieur, L., 2012. Introduction to the biogeochemistry from the oligotrophic to the ultraoligotrophic mediterranean (BOUM) experiment. Biogeosciences 9 (10), 3817–3825.

Orr, J.C., Fabry, V.J., Aumont, O., Bopp, L., Doney, S.C., Feely, R.A., et al., 2005. Anthropogenic ocean acidification over the twenty-first century and its impact on calcifying organisms. Nature 437 (7059), 681–686.

Pinardi, N., Zavatarelli, M., Adani, M., Coppini, G., Fratianni, C., Oddo, P., Simoncelli, S., Tonani, M., Lyubartsev, V., Dobricic, S., Bonaduce, A., 2013. Mediterranean Sea large-scale low-frequency ocean variability and water mass formation rates from 1987 to 2007: A retrospective analysis. Prog. Oceanogr , http://dx.doi.org/10.1016/j.pocean.2013.11.003.

Pinardi, N., Tonani, M., Grandi, A., Santoleri, L., Buongiorno-Nardelli, B., 2007. JRA5: Mediterranean products - Data Analysis Protocol for the Mediterranean Sea, SeaDataNet Project Contract no. 026212, Deliverable 17, pp. 23.

Plancherel, Y., Rodgers, K.B., Key, R.M., Jacobson, A.R., Sarmiento, J.L., 2013. Role of regression model selection and station distribution on the estimation of oceanic anthropogenic carbon change by eMLR. Biogeosciences 10, 4801–4831.

Rivaro, P., Messa, R., Massolo, S., Frache, R., 2010. Distributions of carbonate properties along the water column in the Mediterranean Sea: spatial and temporal variations. Mar. Chem. 121 (1), 236–245.

Sabine, C.L., Tanhua, T., 2010. Estimation of anthropogenic CO_2 inventories in the ocean. Annu. Rev. Mar. Sci 2, 175–198.

Sabine, C.L., Feely, R.A., Gruber, N., Key, R.M., Lee, K., Bullister, J.L., et al., 2004. The oceanic sink for anthropogenic CO2. Science 305 (5682), 367–371.

Schaap, D.M., Lowry, R.K., 2010. SeaDataNet–Pan-European infrastructure for marine and ocean data management: unified access to distributed data sets. Int. J. Digital Earth 3 (S1), 50–69.

Schneider, A., Wallace, D.W.R., Körtzinger, A., 2007. Alkalinity of the Mediterranean Sea. Geophys. Res. Lett 34, L15608.

Schneider, A., Tanhua, T., Körtzinger, A., Wallace, D.W., 2010. High anthropogenic carbon content in the eastern Mediterranean. J. Geophys. Res.: Oceans (1978–2012) 115 (C12), 1–11.

Schneider, A., Tanhua, T., Roether, W., Steinfeldt, R., 2014. Changes in ventilation of the Mediterranean Sea during the past 25 yr. Ocean Sci 10, 1–16.

Taillandier, V., D'Ortenzio, F., Antoine, D., 2012. Carbon fluxes in the mixed layer of the Mediterranean Sea in the 1980s and the 2000s. Deep Sea Res. I: Oceanogr. Res. Papers 65, 73–84.

Tanhua, T., Hainbucher, D., Cardin, V., Álvarez, M., Civitarese, G., McNichol, A.P., Key, R.M., 2013. Repeat hydrography in the Mediterranean Sea, data from the Meteor cruise 84/3 in 2011. Earth Syst. Sci. Data 5, 289–294.

Tanhua, T., Körtzinger, A., Friis, K., Waugh, D.W., Wallace, D.W., 2007. An estimate of anthropogenic CO_2 inventory from decadal changes in oceanic carbon content. Proc. Natl. Academy Sci 104 (9), 3037–3042.

Touratier, F., Goyet, C., 2009. Decadal evolution of anthropogenic CO_2 in the northwestern Mediterranean Sea from the mid-1990 s to the mid-2000 s. Deep Sea Res. I: Oceanogr. Res. Papers 56 (10), 1708–1716.

Touratier, F., Goyet, C., 2011. Impact of the Eastern Mediterranean Transient on the distribution of anthropogenic CO_2 and first estimate of acidification for the Mediterranean Sea. Deep Sea Res. I: Oceanogr. Res. Papers 58 (1), 1–15.

Touratier, F., Guglielmi, V., Goyet, C., Prieur, L., Pujo-Pay, M., Conan, P., Falco, C., 2012. Distributions of the carbonate system properties, anthropogenic CO_2, and acidification during the 2008 BOUM cruise (Mediterranean Sea). Biogeosciences 9, 2709–2753.

Troupin, C., Barth, A., Sirjacobs, D., Ouberdous, M., Brankart, J.M., Brasseur, P., et al., 2012. Generation of analysis and consistent error fields using the Data Interpolating Variational Analysis (DIVA). Ocean Model 52, 90–101.

Velo, A., Pérez, F.F., Tanhua, T., Gilcoto, M., Ríos, A.F., Key, R.M., 2013. Total alkalinity estimation using MLR and neural network techniques. J. Mar. Syst 111, 11–18.

Willmott, C.J., Matsuura, K., 2005. Advantages of the mean absolute error (MAE) over the root mean square error (RMSE) in assessing average model performance. Climate Res 30 (1), 79.